35th Annual International Conference of the IEEE EMBS
Osaka, Japan, 3 - 7 July, 2013

A Compliant Parallel Mechanism for Needle Intervention

Youngjin Moon, *Member*, *IEEE*, and Jaesoon Choi, *Member*, *IEEE*,

***Abstract*— This paper presents a compliant mechanism for fine motion of a medical robot for needle intervention procedure. The concept of this mechanism is created with the purpose of correcting a needle axis by translating a main robot for needle driving when an unexpected slip happens in needle insertion. In order to specify the concept, a planar compliant mechanism is designed so that the mechanism has maximized workspace for some given design condition. A simplified mathematical model for the designed mechanism is derived and then a pose controller is designed to track a desired trajectory in a plane, which is a similar situation that the compliant mechanism translates a needle driving robot to correct the direction of a needle. The simulation result shows good tracking performance.**

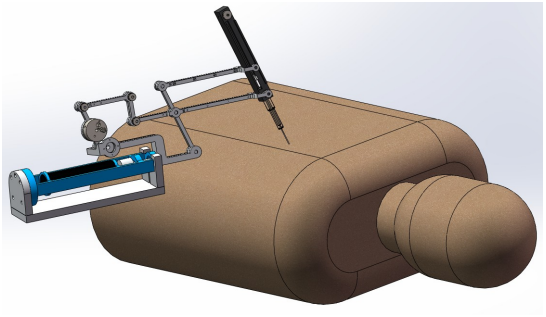

Fig. 1. Biopsy using a robotic mechanism

I. Introduction

Intervention procedure is a relatively new treatment using radiographic equipment and some medical devices such as a needle, catheter, or stent, which can achieve smallest excision and reduced tissue damage or loss, compared with traditional surgery. This procedure is not an exception of the outreach of the robot technology. Many robotics researchers and surgeons have joined their hands with the need for the accuracy and reliability in the medical tasks. The attempts to design and implement robots for intervention, especially needle intervention, can be found in the literature [1], [2].

The robot for needle intervention has basically at least three degree-of-freedom(DOF) motion: two rotations whose axes are perpendicular each other about a pivot point and a translation for needle insertion as shown in Fig. 1. The pivot point, entry point on the patient's body, locates outside workspace of a robot and it is called Remote Center of Motion (RCM). Many researchers have presented various types of kinematic mechanisms with RCM motion such as parallelograms [3], [4], a gimbal or arc [5], [6], a chain transmission [7], double layered mechanisms [8], [9], and parallel mechanisms [10], [11].

However, actual motion of a needle by surgeons and physicians in biopsy is more complicated than aforementioned basic motion by robots. There is an example by the characteristics of skin and soft tissue as shown in Fig. 2. The direction of a needle in ① is toward a lesion detected by a radiological equipment like CT(Computed tomography). Ideal situation could be that the needle reaches the lesion without any skew but the needle often slide on patients' skin, that is ② happens. In order to correct the direction of the needle, three ways, ③-1,2, and 3 in the right side of Fig. 2 can be considered under the assumption that the needle is stiff enough: rotation about a point, backward translation, and forward translation. The latter seems to be feasible while the former two are impractical due to the effect that tissue tightly holds the needle tip. Please note that ③-3 is not pure translation, but combination of translation and rotation for the robot.

This paper presents a robotic mechanism aiding such translation of a robot for intervention. The mechanism is designed as hybrid one so that it can actively translate the robot or passively compensate an unexpected needle motion due to respiration. Following a design issue of the mechanism to be covered, the paper proceeds by deriving dynamic equation, designing a controller, and simulating control performance.

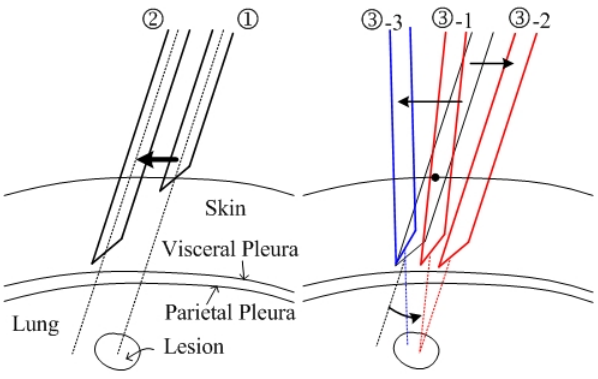

Fig. 2. Concept for correction of needle insertion in lung biopsy

*This work was supported by the Industrial Strategic technology development program, grant number 10041618, Development of Needle Insertion Type Image-based Interventional Robotic System for Biopsy and Treatment of 1-cm Abdominal and Thoracic Lesion with Reduced Radiation Exposure and Improved Accuracy, funded by the Ministry of Knowledge Economy(MKE, South Korea)

The authors are with Medical Engineering Research & Development Center, Asan Institute for Life Sciences, Asan Medical Center and University of Ulsan-College of Medicine, Seoul 138-736, South Korea {youngjin.moon, jaesoon.choi} at gmail.com

TABLE I

OPTIMIZATION RESULT

Optimized values	$[0.9857, 0.5620, 5.4942, 0.6561,$ $0.6837, 1.6453, 4.3917, 0.5448]$
Final fitness	55.5850
Generation	51

II. MECHANISM DESIGN

In order to design a compliant mechanism for both translation of a needle driving robot and compensation of a needle motion, a planar tensegrity-based compliant mechanism in [12] is adopted. The mechanism has hybrid function of both an active manipulator and a passive compliant device using a tensegrity-like structure.

The mechanism is designed considering the following conditions.

1) The mechanism has a shape of a square whose two opposite sides are the top and base platforms.
2) The lengths of the springs and pistons are bounded; they have minimum and maximum lengths.
3) It can have a two-layer structure to avoid interference between the legs.
4) The most left-side joints in both platforms are the origins for both body coordinate systems, respectively.

Under these conditions, the main focus in mechanism design is how to choose positions of the joints on the top and base platform. Each joint should be located so that the mechanism has enough workspace and minimizes the singular area in workspace. This can be thought as a optimization problem. The joints, $\mathbf{p}_1$, $\mathbf{p}_4$, $\mathbf{p}_5$, and $\mathbf{p}_8$, can be chosen from the size of the top and base platforms. Design variables are then defined as $p_{2x}, p_{2y}, p_{3x}, p_{3y}, p_{6x}, p_{6y}, p_{7x}, p_{7y}$ for $\mathbf{p}_2 = [p_{2x},\ p_{2y}]^T$, $\mathbf{p}_3 = [p_{3x},\ p_{3y}]^T$ on the base platform, $\mathbf{p}_6 = [p_{6x},\ p_{6y}]^T$, and $\mathbf{p}_7 = [p_{7x},\ p_{7y}]^T$ on the top platform. The plane of $\{x \in [-10, 15], y \in [-10, 10]\}$ is given as the area to check workspace and singularity. This area is divided into 1000 $\times$ 1000 segments to calculate fitness value for a cost function. The cost function is defined as

$$f_v \quad = \quad \frac{w_a}{c_{ws}} + w_b c^*_{sg} \tag{1}$$

where w_a and w_b are weights, c_{ws} is the ratio of workspace to the total area, $\frac{\#\ of\ workspace\ segments}{\#\ of\ total\ segments}$, and c_{sg} is the ratio of singular points to the total area, $\frac{\#\ of\ singular\ segments}{\#\ of\ total\ segments}$. c^*_{sg} is the value that comes from binary mask operation to the matrix including workspace segments. Workspace can be calculated by kinematics and singular area in the total area can be calculated by checking the condition number of the Jacobian matrix $H = [\$_1,\ \$_2,\ \$_3,\ \$_4]^T$. In this study, H is considered as singular when $cond(H) > 5000$.

The optimization method to minimize f_v is chosen as the typical genetic algorithm [13] because this method is suitable for the situation when the system is given as a non-explicit function which requires pointwise calculation by iteration. In the process, population size is 10, crossover is 0.8, elite count is 2, and $w_a = 10$, $w_b = 1e + 6$ are used.

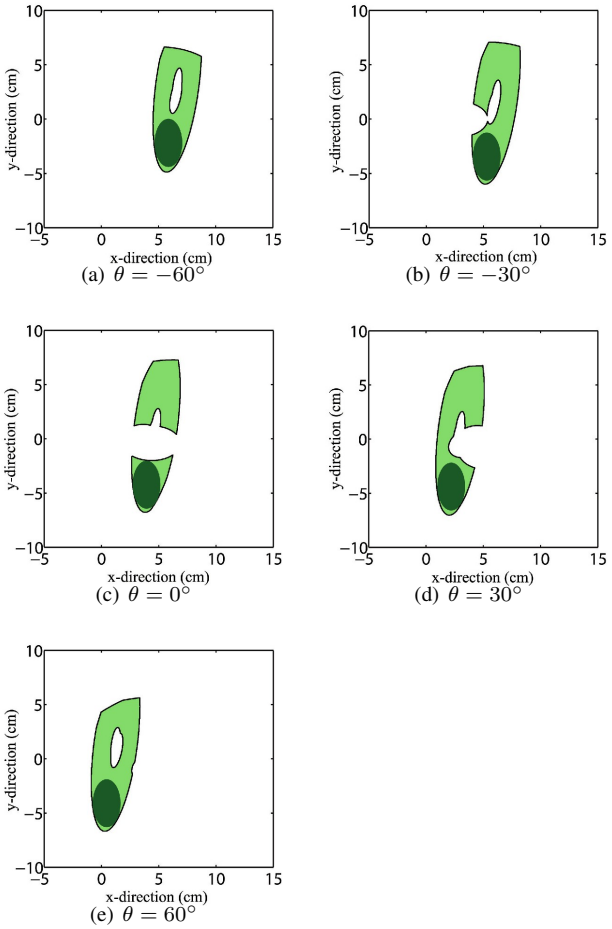

Fig. 3. Workspace for the selected orientation angles

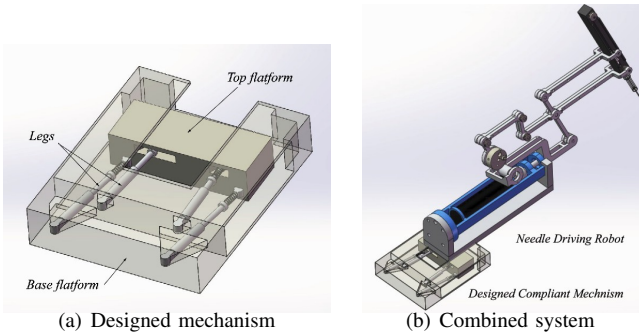

(a) Designed mechanism (b) Combined system

Fig. 4. 3D model of the mechanism

The result for the converged fitness value is shown in Table I. Fig. 3 shows workspace (green area including dark green) for the mechanism. The dark green area means common workspace which can be drawn as ellipse or circle. All the ellipses in Fig. 3 have vertices of (1.25, 0) and (0. 2.25), that is the distances between two vertices 2.5 cm and 4.5 cm for X and Y axes, respectively. This result ensures that the mechanism can move the needle driving robot in the range. A 3D mechanism model whose size is 12cm$\times$15cm$\times$3cm is created as shown in Fig. 4.

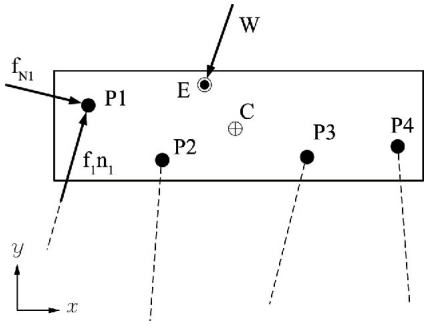

Fig. 5. Top body free body diagram

III. Dynamic Equation

A simplified dynamic model is necessary for this parallel mechanism whose dynamics becomes more complicated by existence of the springs. The approach used in [14] could be helpful to derive the equation. The mathematical model can be divided into two parts: a top platform and leg connectors as shown in Fig. 5 and 6. The entire procedure to derive the equation is omitted due to lack of space.

The resultant equation for a top platform model can be obtained as

$$M_t\ddot{\mathbf{q}} + \mathbf{N} = H\mathbf{f}_P \tag{2}$$

where $M_t \in \mathcal{R}^{3\times3}$ depicts an inertia matrix, $\mathbf{q} \in \mathcal{R}^{3\times1}$ depicts three parameters related to the position and orientation of the top platform, $\mathbf{N} \in \mathcal{R}^{3\times1}$ depicts a nonlinear terms, $H \in \mathcal{R}^{3\times3}$ is a Jacobian matrix, and $\mathbf{f}_P \in \mathcal{R}^{3\times1}$ depicts a vector including force magnitudes acting along the leg line.

The resultant equation for each leg model can be also obtained as

$$M_p\ddot{\mathbf{x}}_a = -K_p(\mathbf{x}_a - \mathbf{x}_s) - B_p(\dot{\mathbf{x}}_a - \dot{\mathbf{x}}_s) - \mathbf{f}_p - \mathbf{f}_r + \mathbf{f}_a \tag{3}$$

where $M_p = diag(m_i) \in \mathcal{R}^{4\times4}$, $B_p = diag(b_{pi}) \in \mathcal{R}^{4\times4}$, $K_p = diag(k_{pi}) \in \mathcal{R}^{4\times4}$, $K = diag(k_i) \in \mathcal{R}^{4\times4}$, and others are the 4×1 vectors which consist of i-th components, for example, $\mathbf{x}_a = [x_{a1}, x_{a2}, x_{a3}, x_{a4}]^T$.

IV. Control Simulation

In order to verify the performance for planar motion of the mechanism, the pose (position and orientation) control simulation is performed. Associating with the mathematical

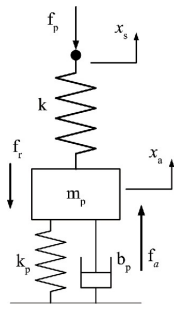

Fig. 6. Free body diagram for a leg

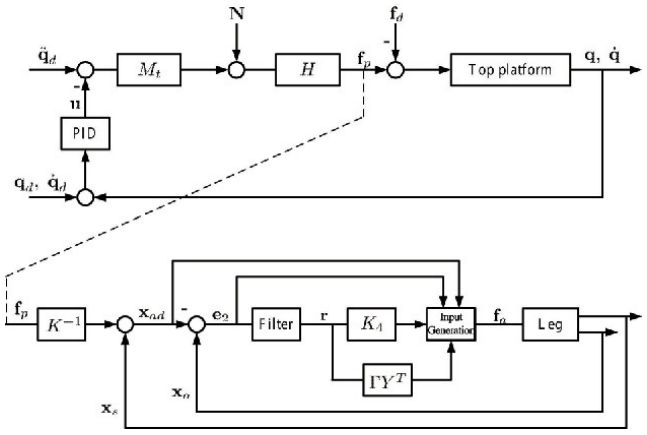

Fig. 7. Control schematic

models described the previous section, a two-stage control is proposed as shown in Fig. 7. This control consists of two levels: PID-computed torque control of the motion of the top platform and adaptive control of the piston in the leg connector. PID control tracks a desired pose using the joint forces along the line of the leg connector, $\mathbf{f}_p$, which is tracked by adaptive control with estimation of uncertain parameters such as stiffness, damping coefficient, and friction coefficient in the piston.

The control law for each part can be designed as

$$\mathbf{u} = -K_1\mathbf{e}_1 - K_2\dot{\mathbf{e}}_1 - K_3\boldsymbol{\epsilon}_1 \tag{4}$$

$$\mathbf{f}_a = -Y\hat{\boldsymbol{\vartheta}} + \mathbf{f}_p + M_p\ddot{\mathbf{x}}_{ad} - \alpha_1 M_p\dot{\mathbf{e}}_2 - K_4\mathbf{r} - \mathbf{e}_2 \tag{5}$$

where K_1, K_2, K_3, and K_4 are gains, $\mathbf{e}_1$ depicts pose error, $Y \in \mathcal{R}^{4\times12}$ depicts a regression matrix, α_1 depicts a constant, $\mathbf{e}_2$ depicts piston displacement error, r depicts a filtered tracking error, and $\boldsymbol{\epsilon}_1 = \int \mathbf{e}_1 dt$.

The desired trajectory and disturbance are given as

$$\mathbf{q}_d = [6\sin(\pi t), 12\sin(0.4\pi t), 5\sin(0.2\pi t)]^T \text{ cm,cm,deg}$$

$$\mathbf{f}_d = 0.01\sin(2\pi t) + 0.005\sin(10\pi t) \text{ N.}$$

The simulation result is shown in Fig. 8 to 13. In Fig. 8, the top platform tracks the desired position and velocity, and the tracking error seems very small after 1 second. Fig. 9 and 10 show piston displacement converges to the desired value and the error, $\mathbf{e}_2$ becomes small. In Fig. 11, parameter estimates converge. Fig. 12 and 13 show control inputs in each level control.

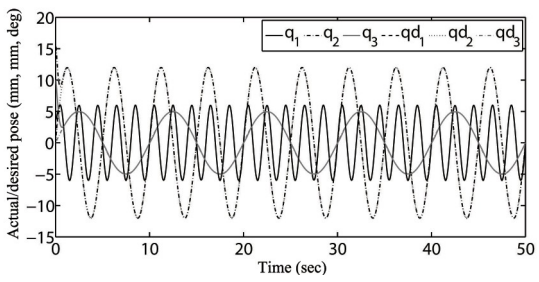

Fig. 8. Position and orientation

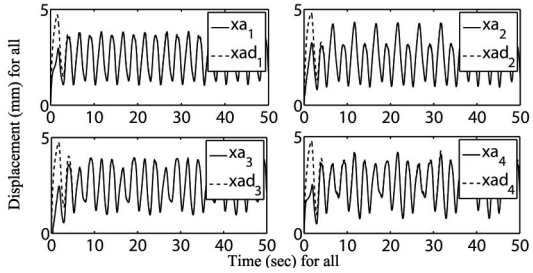

Fig. 9. Piston displacement

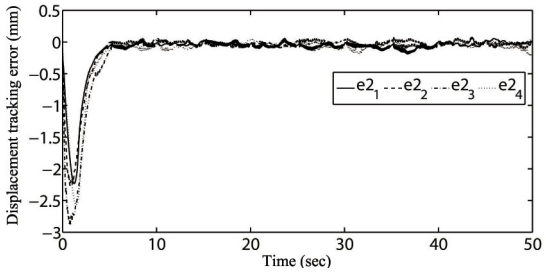

Fig. 10. Piston displacement error

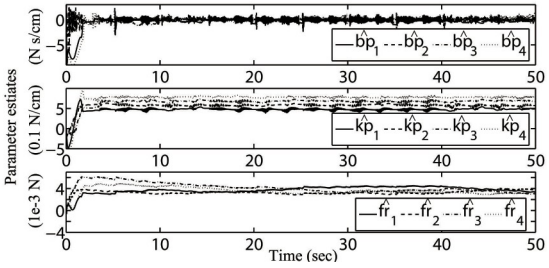

Fig. 11. Parameter estimates

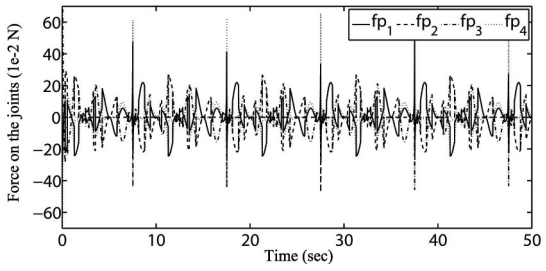

Fig. 12. Intermediate control input at the joint

V. Discussion and Conclusion

The simulation result shows that this type of mechanism, the planar tensegrity-based compliant mechanism can achieve precise motion tracking in a plane for the given condition. That is to say, the mechanism could be useful in translating a needle driving robot to correct a wrong needle axis due to a physical property of skin in robotic biopsy. Meanwhile, there is still room for improvement in the design optimization. It is more reasonable that the performance index is defined as a specific range rather than maximum

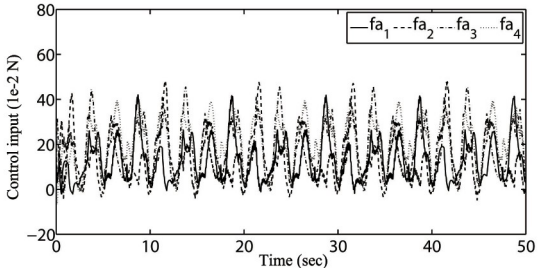

Fig. 13. Control input at the piston

workspace area used in this study. The control performance when a heavy load is associated with the top platform of the mechanism and performance as a passive compliance device should be verified in follow-up research.

References

[1] R. Taylor and D. Stoianovici, "Medical robotics in computer-integrated surgery," *IEEE Transactions on Robotics and Automation*, vol. 19, no. 5, pp. 765–781, 2003.

[2] P. Kazanzides, G. Fichtinger, G. Hager, A. Okamura, L. Whitcomb, and R. Taylor, "Surgical and interventional robotics-core concepts, technology, and design [tutorial]," *IEEE Robotics & Automation Magazine*, vol. 15, no. 2, pp. 122–130, 2008.

[3] A. Melzer, B. Gutmann, T. Remmele, R. Wolf, A. Lukoscheck, M. Bock, H. Bardenheuer, and H. Fischer, "Innomotion for percutaneous image-guided interventions," *IEEE Engineering in Medicine and Biology Magazine*, vol. 27, no. 3, pp. 66–73, 2008.

[4] Y. Kobayashi, J. Hong, R. Hamano, K. Okada, M. Fujie, and M. Hashizume, "Development of a needle insertion manipulator for central venous catheterization," *The International Journal of Medical Robotics and Computer Assisted Surgery*, 2011.

[5] C. Walsh, N. Hanumara, A. Slocum, J. Shepard, and R. Gupta, "A patient-mounted, telerobotic tool for ct-guided percutaneous interventions," *Journal of Medical Devices*, vol. 2, no. 1, pp. 011 007–10, 2008.

[6] X. Chen *et al.*, "Instrument guide for mri-guided percutaneous interventions," Ph.D. dissertation, Massachusetts Institute of Technology, 2010.

[7] D. Stoianovici, L. Whitcomb, J. Anderson, R. Taylor, and L. Kavoussi, "A modular surgical robotic system for image guided percutaneous procedures," *Medical Image Computing and Computer-Assisted Intervention—MICCAI98*, pp. 404–410, 1998.

[8] O. Bebek, M. Hwang, and M. Cavusoglu, "Design of a parallel robot for needle-based interventions on small animals," *IEEE/ASME Transactions on Mechatronics*, vol. 18, no. 1, pp. 62–73, 2011.

[9] B. Schulz, K. Eichler, P. Siebenhandl, T. Gruber-Rouh, C. Czerny, T. Vogl, and S. Zangos, "Accuracy and speed of robotic assisted needle interventions using a modern cone beam computed tomography intervention suite: a phantom study," *European Radiology*, pp. 1–7, 2012.

[10] J. Chung, H. Cha, B. Yi, and W. Kim, "Implementation of a 4-dof parallel mechanism as a needle insertion device," in *2010 IEEE International Conference on Robotics and Automation (ICRA)*. IEEE, 2010, pp. 662–668.

[11] Y. Kobayashi, A. Onishi, H. Watanabe, T. Hoshi, K. Kawamura, M. Hashizume, and M. Fujie, "Development of an integrated needle insertion system with image guidance and deformation simulation," *Computerized Medical Imaging and Graphics*, vol. 34, no. 1, pp. 9–18, 2010.

[12] Y. Moon, C. Crane III, and R. Roberts, "Position and force analysis of a planar tensegrity-based compliant mechanism," *Journal of Mechanisms and Robotics - Transaction of the ASME*, vol. 4, no. 1, pp. 001 004–1–001 004–8, 2012.

[13] D. E. Goldberg and J. H. Holland, "Genetic algorithms and machine learning," *Machine learning*, vol. 3, no. 2, pp. 95–99, 1988.

[14] J. Merlet, *Parallel robots*. Springer-Verlag New York Inc, 2006.